Facile synthesis of zinc oxide nanoparticles loaded activated carbon as an eco-friendly adsorbent for ultra-removal of malachite green from water

Esra Altıntıg[1], Merve Yenigun[1], Ahmet Sarı[2,3], Huseyin Altundag[1], Mustafa Tuzen[4,5], Tawfik A. Saleh [6*]

[1]*Sakarya University, Art and Science Faculty, Chemistry Department, 54187 Sakarya, Turkey*
[2]*Karadeniz Technical University, Engineering Faculty, Metallurgical and Material Engineering Department, 61080 Trabzon, Turkey*
[3]*Center of Research Excellence in Renewable Energy (CORERE), Research Institute, King Fahd University of Petroleum & Minerals, Dhahran, 31261, Saudi Arabia*
[4]*Tokat Gaziosmanpasa University, Art and Science Faculty, Chemistry Department, 60250 Tokat, Turkey*
[5]*King Fahd University of Petroleum and Minerals, Research Institute, Center for Environment and Water, Dhahran, 31261 Saudi Arabia*
[6] *Department of Chemistry, King Fahd University of Petroleum and Minerals, Dhahran, 31261, Saudi Arabia*
Corresponding Author: tawfikas@hotmail.com; tawfik@kfupm.edu.sa

Abstract

Green synthesis ultrasonic method is reported for the preparation of zinc oxide nanopartilces loaded on activated carbon derived from coffee waste. The zinc modified AC was used effectively for the elimination of malachite green (MG) from wastewater. The examined batch adsorption parameters are; initial pH (2-9), sorbent amounts (0.10-0.50 g/100 mL), mixing time (5-120 min), MG concentrations (25-300 mg/L) and temperature (298-318 K). The XRD, SEM/EDS, and FT-IR analysis techniques were conducted to describe the chemical structure as well as surface morphology of $Zn(OH)_2$-AC composite. The results demonstrated that the adsorption capacity of $Zn(OH)_2$-AC composite was improved with incremental of the initial dye concentration, pH, and temperature, and decreased as the $Zn(OH)_2$-AC composite dose was increased. The Langmuir isotherm model (R^2 = 0.97) showed better conventionality than the Freundlich model (R^2 = 0.80) with a maximum removal capacity of 303.03 mg/g at 318 K and pH 7.0. The kinetic results revealed that the equilibrium data well follow the pseudo-second-order model. The thermodynamic investigations indicated the spontaneous and

endothermic removal of MG. The cycling test exhibited that the developed $Zn(OH)_2$-AC composite had virtuous repeatable adsorption/desorption performance particularly until the fourth cycle. In addition to comparatively shorter adsorption time, relatively high adsorption capacity, reasonable reuse performance, and being of cost-effective and eco-friendly of the developed $Zn(OH)_2$-AC composite make it economic, effective and hopeful adsorbent for cleaning MG containing wastewaters.

Keywords: Zinc hydroxide composite, Malachite green, Kinetic and isotherm, Coffee waste, Adsorption, Ultra removal

1. Introduction

Dyes- containing wastewaters are among the important contaminants due to the ecological problems that they will cause. 10.000 various types of dyes and an average of 700.000 tons of dye are being used around the world (Senthilkumaar et al., 2006). Dyestuffs cause toxic, carcinogenic, and aesthetic problems in aquatic environments (Pharma et al., 2011). Reactive dyes are the most commonly used dyes that are used in the textile industry because of their luminescent structures, fast application, and low cost (Ahmad and Alrozi, 2011). Reactive dyestuffs are not biodegradable because of their solubility feature in the water and azoic structure. Dyes in the wastewaters are being removed by using different traditional methods such as bio-adsorption/adsorption (Altintig et al., 2018; Wangi and Zhu, 2007; Yu et al., 2017; Pereira et al., 2003; S. Dashamiri et al., 2016; Saleh 2020a,b), chemical oxidation (Wang et al., 2015) and magnetic separation (Huang, 2017). The removal of organic dyes using different kinds of bio-based-AC. When these methods are compared, the most preferred method is adsorption because of easy use (Ip et al., 2009; Lin et al., 2017). The adsorption process comes into prominence because it provides high-quality output water on the removal of the dissolved organic contaminants as dyes (Walker and Weatherley, 1997; Zhang et al. 2019; Zhu et al. 2020). In recent years researchers modified the nano-structure materials to

increase the surface areas of activated carbons (ACs) and their adsorption capacities. The use of hydroxylated metal nanoparticles such as copper (II) oxide (Mazaheri et al., 2015), ruthenium and copper covered zinc sulfide (Asfaram et al., 2015), zinc oxide nano particles (Azad et al., 2015) have been preferred as chemical activating agents of the different kinds of ACs used as adsorbents due to some advantages like high selectivity and various reactive centers (Dashamiri et al., 2017; Sadeghi et al., 2012). Moreover, various methods have been tried to activate these modification processes and adsorbents. Some of them are acid cavitation, thermal activation, and acoustic cavitation. Acoustic cavitation is based on the application of ultrasonic radiation to the aquatic environment. When ultrasound was spread in the aquatic environment, cavitation bubbles were created in the aquatic environment with the effect of the high ultrasonic pressure. These bubbles grow up to an unbalanced dimension and precipitate introverted (Jing et al., 2011). As the diameters of the bubbles created at lower frequencies at around 20 kHz are greater relatively, the intensity of the hydro-mechanical shear forces created during the cavitation precipitation at lower ultrasonic frequency is maximum. This mechanism of the acoustic cavitation can be used to increase the activation of adsorbents and adsorption capacities (Breitbach and Bathen, 2001).

Even though numerous countries have prohibited the usage of MG because of its serious harmful effects, it has been still used in some industrial activities such as fish farming, for dyeing of textile products due to its being cost-effective and easily obtainable (Ramaraju et al., 2014). With remediation purpose of MG-polluted wastewaters, some AC based-adsorbents were modified with ZnO or $Zn(OH)_2$ nanoparticles because of increased number of oxygen-containing functional groups and structural bonding of zinc to the surface of AC. Moreover, compared with the non-modified AC, Zn element on the surface improves the adsorption selectivity of AC to the target molecules and expanding the interlayer spacing of adjacent AC planes (Liu et al., 2020). With this regard, $Zn(OH)_2$ nanoparticle-loaded AC

(Bazrafshan, et al., 2015), bio-based magnetic AC (Wangi and Zhu, 2007) chemical functionalized AC (Ghasemi et al., 2016), ZnO-loaded AC (Ghaedi et al., 2016), coconut coir based-AC (Askari et al., 2017) were reported to eliminate MG from water. In addition, although there are a few studies on $Zn(OH)_2$ loaded AC using different methods in the literature (Bazrafshan et al.,2015; Ghasemi et al., 2016; Mosayebi et al., 2015; Mosayebi and Azizian, 2016). By considering the literature survey, it can be remarkably noted that development of a novel low-cost, economic and facile synthesizable zinc acetate-activated carbon (AC) for effective cleaning of aqueous solutions from MG pollutant is still needed. In this sense, the green and facile synthesis of coffee waste-based AC/$Zn(OH)_2$ composite was carried out by means of ultrasonic cavitation method and then evaluated for removal of MG from aqueous solutions for the first time in this study. A series of instrumentation techniques was conducted for characterization of the adsorbent using XRD, FT-IR, and SEM/EDS, analysis. In addition, adsorption isotherm modeling and reusability cycling test, as well as thermodynamic and kinetic examinations of the adsorption method were applied.

2. Material and Method

2.1. Material

AC was produced from coffee wastes in this study. Sodium hydroxide (NaOH), zinc acetate (Zn $(CH_3COOH)_2$), and hydrochloric acid (HCl), and MG were supplied from Merck (Darmsadt, Almanya). The MG ($C_{52}H_{54}N_4O_{12}$; MG_w: 329.46g/mol) stock solution was prepared as 1000 $mg.L^{-1}$ and the dilution process was used to prepare solutions with required concentrations. The pH of the solutions was adjusted by 0.1 M HCl or NaOH solution. All chemical agents used in the work were of analytical grade.

2.2. Preparation of coffee waste based-AC adsorbent and its modification with $Zn(OH)_2$ nanoparticles

Initially, AC was produced from coffee wastes in this study. An amount of coffee wastes (CW) was taken from coffee markets at a Sakarya, Turkey province. It was impregnated with 85%V/V H_3PO_4 with a ratio of 1:1 and put into a tube furnace at 700 °C for 60 min to become AC (CWAC). The CWAC was washed with water until its filtrate was neutral.

In the second step, the produced coffee waste based-AC adsorbent was modified by $Zn(OH)_2$ nanoparticles via the in-situ process. For this aim, 50.0 mL of 0.05 M zinc salt was mixed with 50 mL of 0.1 M NaOH solution at room temperature. After adding 2 g AC, the mixture was shaken in the ultrasonic bath for 15 min at 200 W power. The ultrasonic activation of AC was performed using (Elma brand, E 30 H) model ultrasonic bath. In the next step, the mixture was centrifuged for about 600s at 6000 rpm. It was then washed with water and ethanol. The obtained $Zn(OH)_2$-AC composite was kept in the oven to dry. This nanomaterial was sieved and the particles with a size between 180-212 μm were used in batch adsorption runs.

2.3. Analytical measurements

SEM/EDS analysis photographs were taken under a high vacuum at 20 kV using Jeol JSM-6060LV brand instrument. Au cover processing was performed in order to provide conductivity property to $Zn(OH)_2$-AC composite sample. Images were recorded between 1.000x and 300.000x zoom and 50 μm-200 nm resolution. The EDS analysis was displayed by focusing on a specific point on the scanned image area of the sample. FT-IR spectrum of the adsorbent was obtained using a Perkin Elmer model spectrometer. The ultraviolet and visible light (UV-Vis) measurements were carried out by Shimadzu UV-2600 model Spectrophotometer. The measurement range was taken as 617 nm. pH of each solution was recorded with Mettler TOLEDO Seven Compact device. The crystal structures of the samples were identified with a Rigaku model X-Ray diffractometer (XRD) in 2θ angle range of 10-80°. The thermal degradation stability of the produced AC and $Zn(OH)_2$-AC samples was

investigated using a NETZSCH-STA 449 F1 model Thermogarvimetry analysis (TGA)/Differential thermogravimetric analysis(DTA) instrument. The samples were heated with in nitrogen atmosphere from room temperature to 1000 °C with a heating rate of 10 ° C/min.

2.4. Adsorption and desorption studies

The solutions of MG dye were prepared from the stock solution (1000 mg/L) by dilution. 100 mL aqueous solution was used for each adsorption run from the water. The influence of contact time (5-120 min), initial pH (2-9), adsorbent amount (0.10- 0.50 g/100 mL), temperature (298-318 K) and dye concentration (25-300 mg/L) on the removal of MG. The mixing process was done using a temperature adjusted-shaker at 150 rpm. The mean values obtained after repeated three times were taken into account. The equilibrium concentrations of MG the removal percentage were calculated using Eq. (1-2):

$$q_e = \frac{(C_o - C_e)}{m} xV \quad (1)$$

$$Removal\ (\%) = \frac{(C_o - C_e)}{C_o} x100 \quad (2)$$

Where, q_e is the equilibrium concentration of removed MG onto $Zn(OH)_2$-AC composite (mg/g). C_o and C_e is initial (mg/L) and equilibrium concentration of MG at equilibrium time (mg/L), respectively. *V* and *m* are solution volume (mL) and adsorbent mass (g).

The desorption efficiency of MG was investigated using six different concentrated-eluents: 0.05 M NaOH, 0.1 M NaOH, 0.2 M NaOH, 0.05 M HCl, 0.1 M HCl and 0.2 HCl. 0.1 g of adsorbent was agitated for 60 minutes for MG concentration of 100 mg L^{-1} at a shaking rate of 150 rpm for 2 hours at 298 K. The separated adsorbent from MG solution was washed with purified water and dried in the oven at 60 °C. Before each desorption cycle, MG adsorption

yield (%) was determined as mentioned above. The desorption yield (%) was (Wang et al., 2016).

$$Desorption(\%) = \frac{C_d}{C_a} x100 \quad (3)$$

Where C_d and C_a are desorption and adsorption equilibrium MG concentration (mg L^{-1})

3. Results and discussion

3.1. Characterization results

XRD results of AC and $Zn(OH)_2$-AC composite before and after dyestuff adsorption were evaluated, **Figure 1.** In the diffraction pattern of AC, the large peak in a range of 20 and 30° corresponds to the amorphous phase and the low peak at 2θ value of 39.04° represents the crystalline phase of AC.

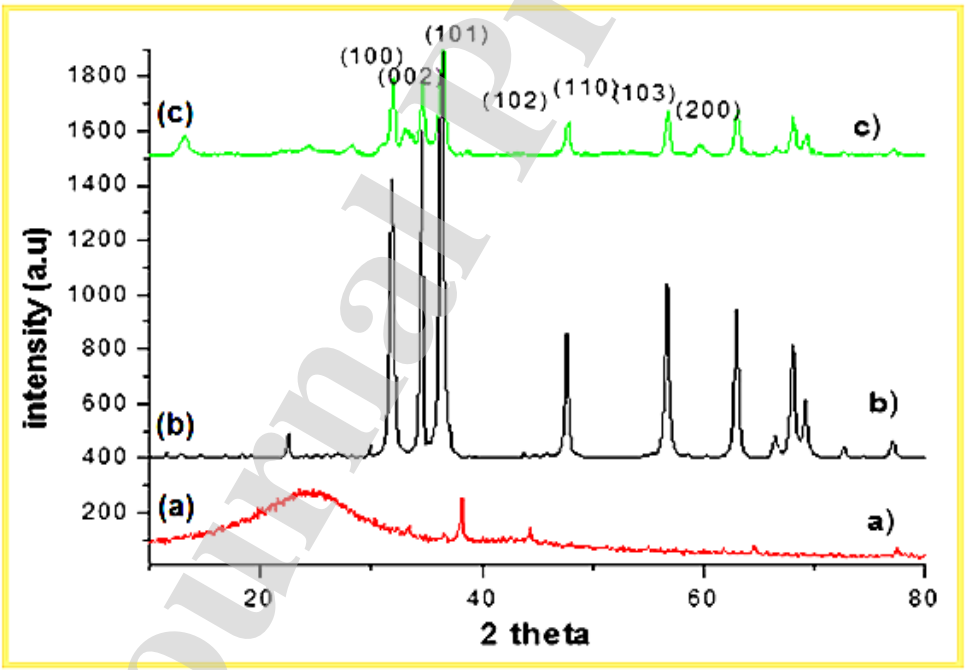

Figure 1. XRD diffraction patterns of **(a)** AC **(b)** $Zn(OH)_2$-AC composite **(c)** $Zn(OH)_2$-AC composite after MG adsorption

As seen from the pattern of $Zn(OH)_2$-AC composite before MG adsorption, the peaks with crystal lattice of 100, 002, 101, 102, 110, 103, 200 correspond to the 2θ value of 32.03, 36.65,

38.27, 48.20, 57.55, 62.33 and 68,76°. On the other hand, it can be seen all main characteristic peaks belonged to AC and $Zn(OH)_2$ are present in the diffraction pattern of $Zn(OH)_2$-AC composite after MG adsorption. Moreover, the sharpness of these peaks was decreased due to the dye adsorption.

Figure 2 shows the FTIR spectrums of AC, $Zn(OH)_2$-AC composite before and after MG adsorption. There are three small absorption bands observed at 1428, 1602, and 887 cm^{-1} corresponding to CH bending vibrations, C=C stretching vibrations, and CH out-of-plane bending vibrations, **Figure 2(a)**. The spectrum of the $Zn(OH)_2$-AC composite indicates peaks at about 3720 and 3390 cm^{-1} are ascribed to the stretching bands of the OH group, **Figure 2(b)**. The minor peaks at about 1426, 1580, and 775 cm^{-1} corresponding to stretching and bending and out-of-plane bending vibrations of CH, C=C, and CH groups of AC components of the adsorbent mentioned above. The peaks at about 1700 and 1070 cm^{-1} are owing to the C=O and C-O stretching vibrations of the acetate group, respectively (Sharma et al., 2012).

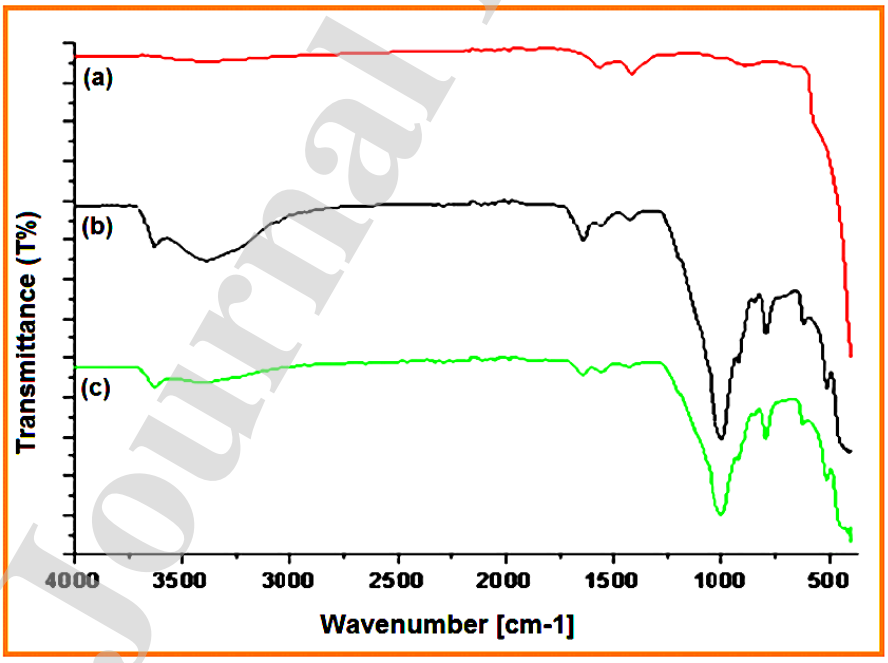

Figure 2. FTIR spectrums of **(a)** AC **(b)** $Zn(OH)_2$-AC composite **(c)** $Zn(OH)_2$-AC composite after MG adsorption

The adsorption peak at 800 and 550 cm^{-1} wave number shows the Zn-O tension in the ZnO cage. The adsorption peak at the 453 cm^{-1} is regarded as the bending vibration of Zn-O in the ZnO cage (Sohail et al., 2017). On the other hand, the spectrum of $Zn(OH)_2$-AC composite includes the absorption signals regarding all of the components of AC after MG adsorption, **Figure 2(c).** Moreover, the little changes in the wavenumber of the peaks were due to the physicochemical attractions between MG and the functional groups of $Zn(OH)_2$-AC composite. By considering all FT-IR findings, it could be concluded that the MG adsorption on the surface of $Zn(OH)_2$-AC composite was accomplished. **Figure 3(a-c)** displays the SEM images of AC $Zn(OH)_2$-AC composite and $Zn(OH)_2$-AC composite after MG adsorption. As can be seen from **Figure 3(a)**, the surface of AC consists of microparticles with arbitrary geometry and their size particles is greater than 10 µm.

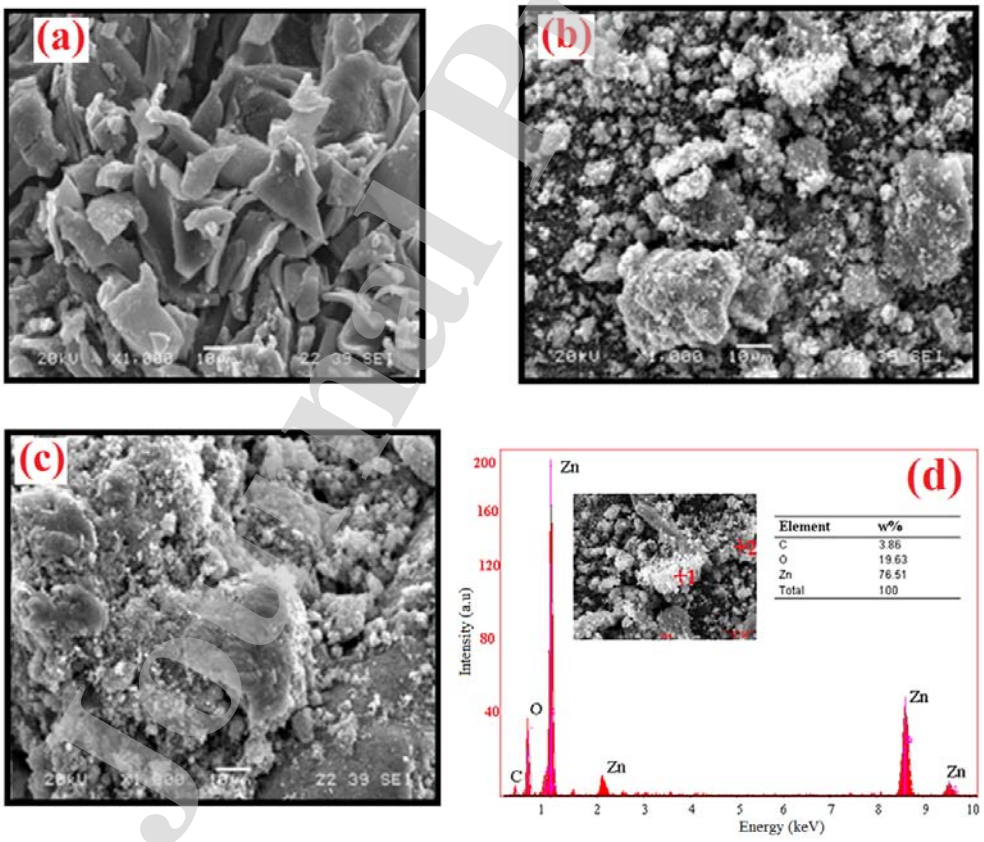

Figure 3. SEM photographs of **(a)** AC **(b)** $Zn(OH)_2$-AC composite **(c)** $Zn(OH)_2$-AC composite after the adsorption **(d)** EDS results of $Zn(OH)_2$-AC composite

Moreover, the existence of holes among these particles can be observed, which can penetrate dye pollutants. The surface structure of the AC was considerably changed because it is covered homogenously with zinc $Zn(OH)_2$ nanoparticles (seen as white color), **Figure 3(b)**. Following the adsorption (**Figure 3(c)**), the surface of $Zn(OH)_2$-AC composite was covered with MG. By taking account of these results, it can be remarkably noted that that the MG was effectively adsorbed on $Zn(OH)_2$-AC composite. Similar microstructures were reported for nano-ZnO/pollen composite for dye removal (Tzvetkov et al., 2017). In addition, **Figure 3(d)** demonstrates the EDS analysis results of $Zn(OH)_2$-AC composite. As detected from spectral data, the weight fractions of C, O, and Zn in the produced adsorbent were found as 3.86, 19.63, and 76.51%.

TGA and DTA analyses results were examined to determine thermal degradation temperature range of both AC and Zn $(OH)_2$ -AC samples as shown in **Figure 4**.

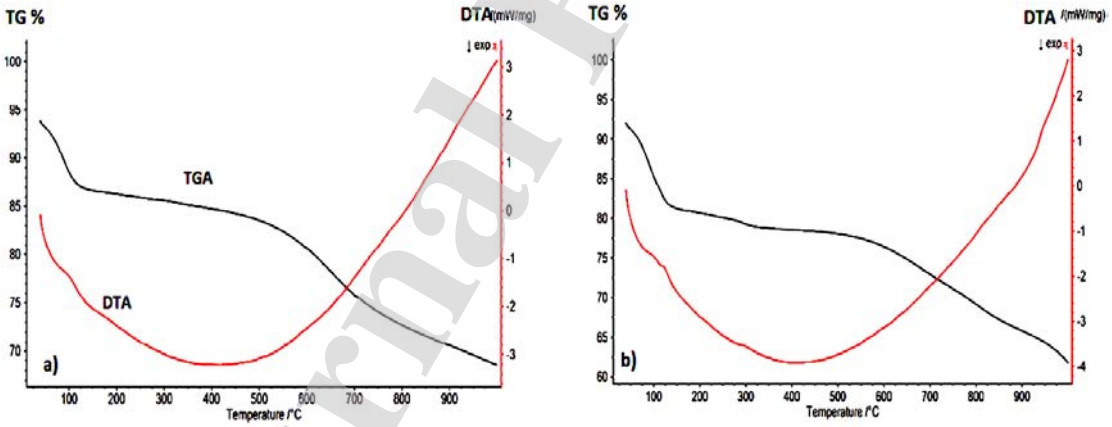

Figure 4. TGA and differential thermogravimetric analysis **(a)**AC **(b)**$Zn(OH)_2$-AC composite

As seen in **Figure 4**, the degradation step in temperature range of 25-120 °C is corresponding to the evaporation absorbed water as the other degradation is step is continuing over 900 °C. On the other hand, the thermal decomposition stage between 25 and 120 °C is attributed to the weight loss of the absorbed water into AC part of the composite. The degradation stage at

120-300 °C is associated with the thermal decomposition of $Zn(OH)_2$ nanoparticles and the rest stage/or stages is regarded with thermal degradation of AC composite.

3.2. pH influence on MG removal yield

pH is considered one of the most imperative factors that influence the surface charge intensity of the adsorbent and diluted ion concentration in solution. Thus, it affects implicitly the adsorption capacity (Behzad et al., 2015). The influence of pH on MG adsorption on $Zn(OH)_2$-AC composite was studied with 0.1 g/100 mL dose at 298 K for 25, 50, and 150 mg/L dye concentrations. The dependency of MG removal yield of $Zn(OH)_2$-AC composite on the pH of the solution is demonstrated in **Figure 5.** The elimination of MG in acidic conditions is relatively lower (in the range of 72-81%) compared to the basic conditions. It could be due to the occupation of H^+ ions onto the adsorbent surface and thus decreasing MG retention (Senthilkumaar et al., 2005). The removal yield of MG was increased as the solution pH was increased. MG adsorption in the cases the pH≥5 for the selected MG concentrations is higher than the adsorption in acidic pH environment. It was because the surface of the adsorbent was negatively charged that allowed much more electrostatic attraction and thus increased MG adsorption. Moreover, the adsorption was almost stabilized after pH 7 and higher. pH 7 was identified as the optimum value for the highest adsorption capacities in all concentrations. Similar results can be found for MG adsorption onto bamboo leaf ash (Dessyntha and Priwidyanjati 2017), using pea shells (Khan et al., 2014) and wood apple shell (Sartapea et al., 2017).

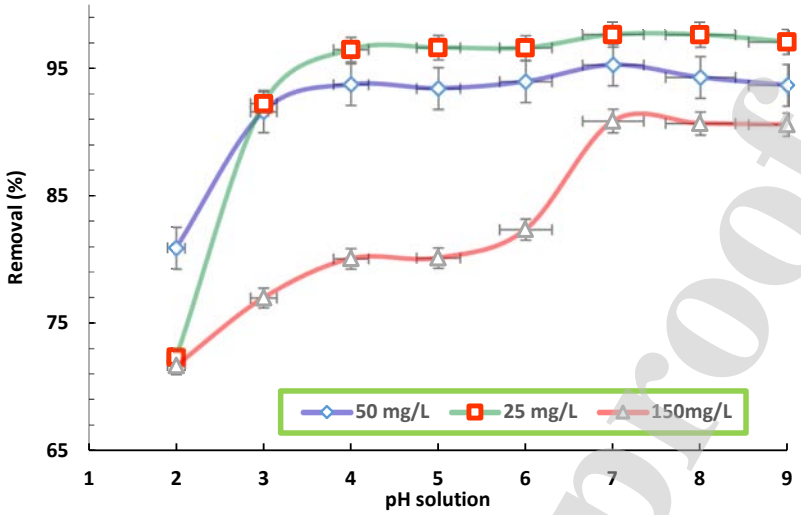

Figure 5. The effect of MG removal yield on the pH of the solution (Initial MG concentration: 50, 100, 150 mg/L, temperature: 298 K, adsorbent dose: 0.1 g/100 mL).

3.3. Mixing time effect on MG removal yield

Adsorption continues until the dynamic equilibrium has occurred between concentration in the solution and adsorbate concentration. There is an identified distribution between the diluted solid and liquid phases. The distribution ratio is the measurement of the equilibrium situation in the adsorption process. To identify the adsorption equilibrium, the solute amount adsorbed in the unit weight of solid adsorbent against the remaining concentration in the equilibrium time at the constant temperature is presented in the graphic (Gupta et al., 2011). To define the adsorption equilibrium time, six different mixing times were studied at different concentrations of the dye, pH 7, 298K, and 0.1 g/100 mL adsorbent dose, **Figure 6.** It was identified that the adsorption equilibrium time started to become constant after 30 min for 3 different concentrations. Moreover, for all studied initial MG concentrations, it was decided that the optimized mixing time was 60 min.

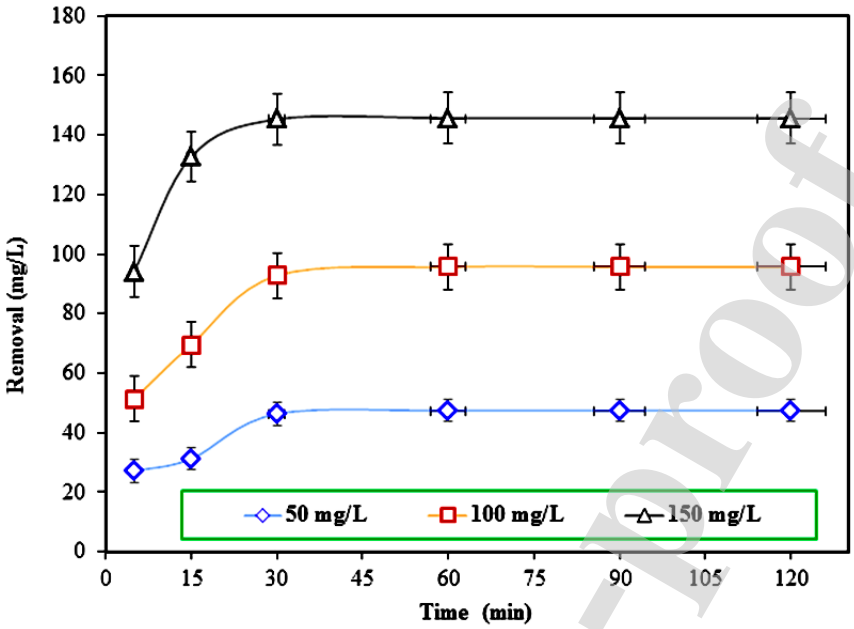

Figure .6 The mixing time effect the removal yield of MG (Temperature: 298 K and pH: 7)

3.4. Adsorbent dose effect on MG removal yield

The adsorbent dose is one of the chief limits that affect the removal yield. In the case the adsorbent dose is insufficient, maximum removal yield may decrease and, otherwise, it is high, flocculation may occur in the solution. Both cases influence adsorption negatively (Xiao et al., 2010). In this study, the adsorbent dose was taken as four different values as 0.5, 0.1, 0.2, and 0.5 g/100 mL at different concentrations of the dye, pH 7, and 298K (**Figure 7)**. The removal yield was over 90% for all examined initial MG concentrations with an increase of adsorbent dose. The highest yield was observed for 0.3 g/100 mL dose and 50 mg/L initial MG concentration. Moreover, there was no increase above 0.3 g/100 mL dose for 100 mg/L initial concentration. The lowest yield was determined as 87.5% for 0.5 g/100 mL dose at 100 mg/L concentration. By considering these results, the optimum sorbent mass was taken as 0.1 g/100 mL for the next batch adsorption experiments.

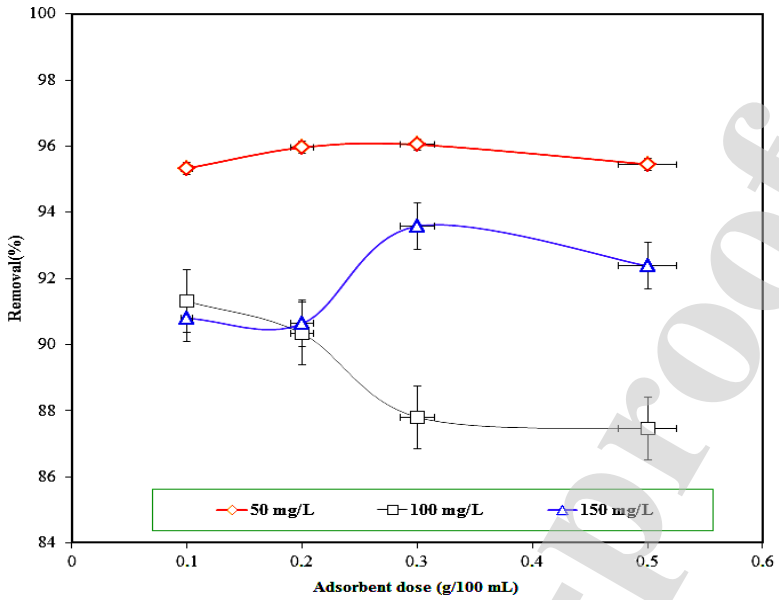

Figure 7. Adsorbent dose effect on the removal yield of MG (temperature: 298 K and pH:7)

3.5. Initial MG concentration effect on MG removal yield

The dependency of removal yield on the initial MG concentration was also investigated at 298-318 K, pH 7, and 0.1 g/L dose. The results obtained for six different initial MG concentrations, 25, 50, 75, 100 150, and 300 mg/L, are presented in **Figure 8.**

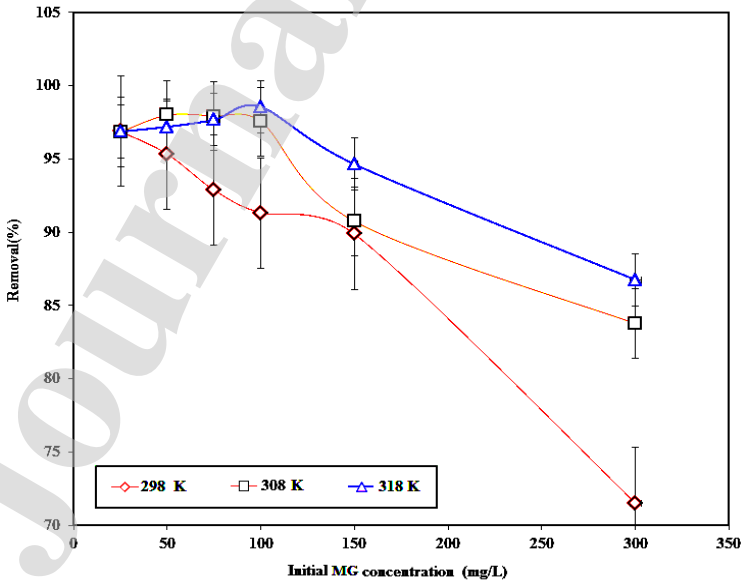

Figure 8. The initial MG concentration effect on the removal yield of MG (temperature: 298-318 K, pH: 7, adsorbent dose: 0.1 g/100mL).

In **Figure 7,** it was observed that the adsorption yield was dropped with an increase of initial MG concentration for the studied temperatures. Moreover, the removal yield was the same value (96.9%) for 25.0 mg/L dye at 298 K while it was found to be 71.5, 83.8, and 86.8%, respectively at 298, 308, and 318 K.

3.6. Temperature effect on the amount of removed MG

The temperature effect on the amount of removed MG was searched at three different temperatures, 298, 308, and 318 K for pH 7, 0.1 g/100 mL dose, and 100 mg/L initial concentration of dyestuff. **Figure 9** displays the effect of temperature on the removal of MG.

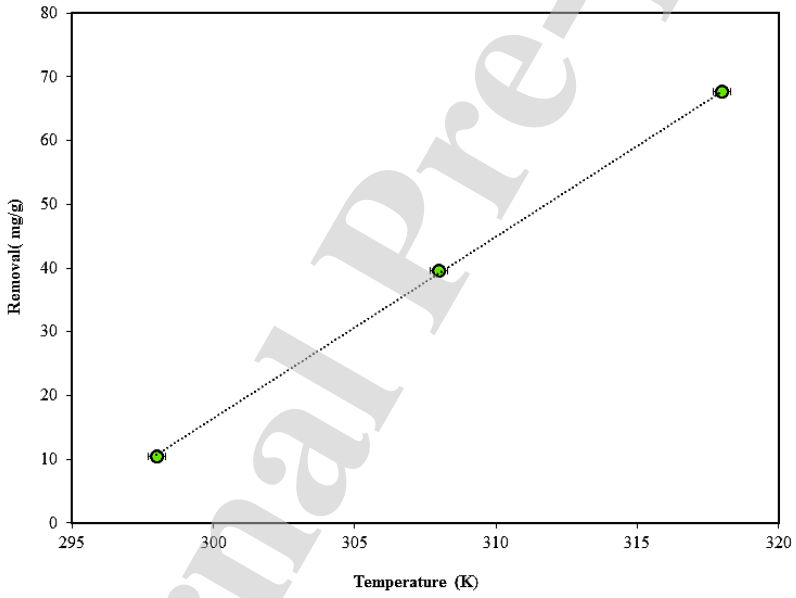

Figure 9. Temperature effect on the amount of removed MG

As seen from the graph, the amount of removed MG was linearly improved with rising temperatures. The quantity of adsorbed MG was determined as 10.5, 39.7, and 67.7 mg/g, at about 298, 308, and 318 K. This result was due to the enhanced mobility of the MG molecules from solution to the surface of the adsorbent through the temperature (Almeida et al., 2009).

3.7. Adsorption thermodynamics

Changes in entropy (Δ*S*°), enthalpy (Δ*H*°), and Gibbs free energy (Δ*G*°), parameters were defined by Eqs. (3-6). The Δ*G*° parameter was calculated by considering the distribution constant (K_D) at equilibrium time.

$$\Delta G^o - RTlnK_D \quad (4)$$

$$ln\ K_D = \frac{b_2}{b_1} \quad (5)$$

$$\Delta G^o = \Delta H^o - T\Delta S^0 = -RTlnK_D \quad (6)$$

$$lnK_D = -\frac{\Delta H^o}{RT} + \frac{\Delta S}{R} \quad (7)$$

The Δ*H*° and Δ*S*° functions were determined from the slope and intersection point of ln K_D versus 1/T plot. Here, b_2 means the adsorption capacity (mg/g) at equilibrium time as b_1 signifies remaining dyestuff concentration (mg/L) in a liquid phase at equilibrium time. *T* and *R* are temperature (*K*) and gas constant (8.314 J/mol.K), (Arias and Sen 2009).

The values of the thermodynamic parameters were calculated, **Table 1.** As seen from this table, the negative Δ*G*° expresses the spontaneity of MG adsorption onto $Zn(OH)_2$-AC composite as its high negative value with increasing temperature means more suitability of the adsorption process (Sara and Tushar, 2012). Thus, the MG adsorption was more favorable at 318 K relative to 298 and 308 K. The positive Δ*H*° demonstrates that the adsorption of MG has an endothermic nature. Moreover, the positive ΔS° specifies the increased randomness at the adsorbent-liquid interface through the removal (Sara and Tushar, 2012). The similar adsorption Positive ΔS° value demonstrates that the randomness on the solid-liquid interface increased during the adsorption The similar adsorption characters were reported for the adsorption congo red from water over pine cone powder (Sara and Tushar, 2012) and the adsorption of three basic dyes onto peat (Allen et al., 2004).

316 **Table 1.** Thermodynamic parameters calculated/determined for
317 MG adsorption onto $Zn(OH)_2$-AC composite

T (K)	ΔG° (kJ/mol)	ΔH° (kJ/mol)	ΔS° (J/mol K)
298	-5.82		
308	-9.42	73.74	0.267
318	-11.13		

318

319 ***3.8. Adsorption isotherms***

320 To identify the adsorption type and determine the maximum removal capacity of the
321 developed adsorbent for MG removal, the equilibrium data was modeled using Langmuir and
322 Freundlich isotherm equations. The Langmuir model known as type-I isotherm suggests
323 an asymptotic methodology for monolayer coverage of the adsorbent surface containing a
324 finite number of adsorption sites. When the adsorption is achieved equilibrium, adsorption
325 capacity is reached a maximum (Dawood and Sen, 2012). The linear formulation of this
326 model can be given as follow:

327 $$\frac{C_e}{q_e} = \frac{1}{q_m K_L} + \frac{1}{q_m} Ce \qquad (8)$$

328 Where C_e is the adsorbate concentration following the adsorption (mg/L), q_e is adsorbed
329 amount onto adsorbent (mg/gr), K_L is isotherm coefficient (L/mg), q_{max} is max sorption
330 capacity (mg/g).

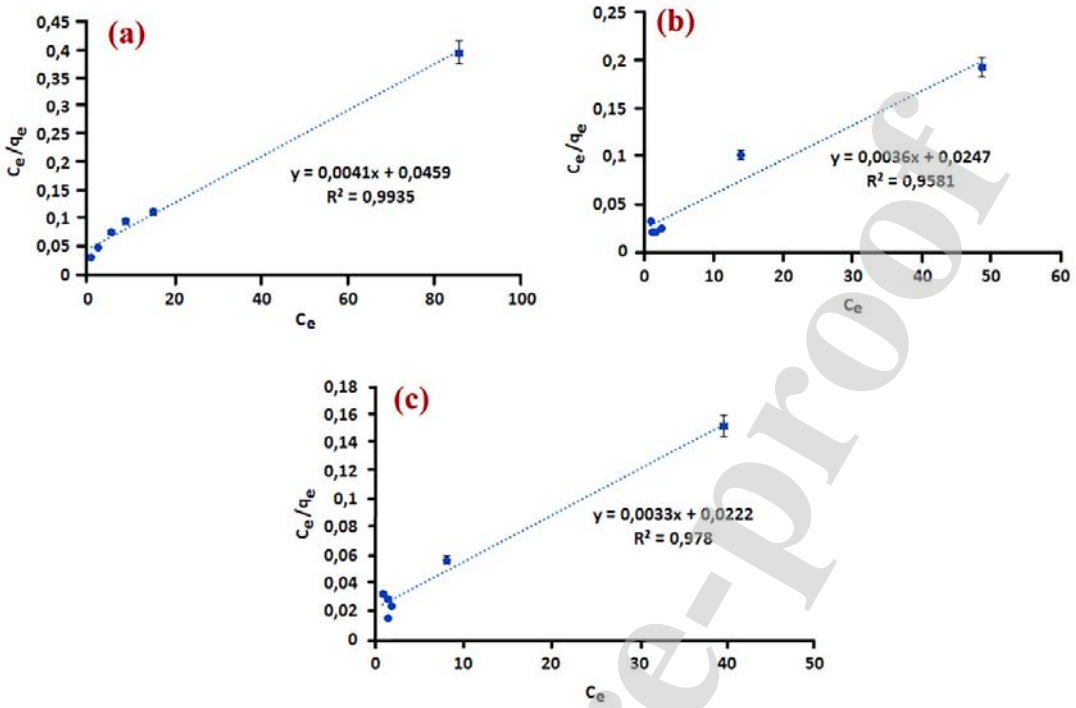

Figure 10. Langmuir isotherm plots obtained **(a)** 298 K; **(b)** 308 K and **(c)** 318 K)

The equilibrium results are in agreement with the Langmuir isotherm plots (**Figure 10**) because of the high correlation coefficient (R^2), 0.99, 0.96, and 0.98 with at 298, 308, and 318 K, respectively. Moreover, q_m and the K_L of $Zn(OH)_2$-AC composite for MG were determined as 243.90, 277.78, and 303.03 mg/g and 0.09, 0.15, 0.15 L/mg, respectively.

The Freundlich isotherm model assumes the multilayer covering of the adsorbent surface by adsorbate molecules (Ozdemir, et al., 2006). The linear formulation of this model is presented below:

$$lnq_e = lnK_f + \frac{1}{n}C_e \quad (9)$$

where q_e is concentration at equilibrium (mg/g) of adsorbate onto the surface of the adsorbent, C_e is adsorbate (mg/L) in solution, and Freundlich's constants are K_f and n.

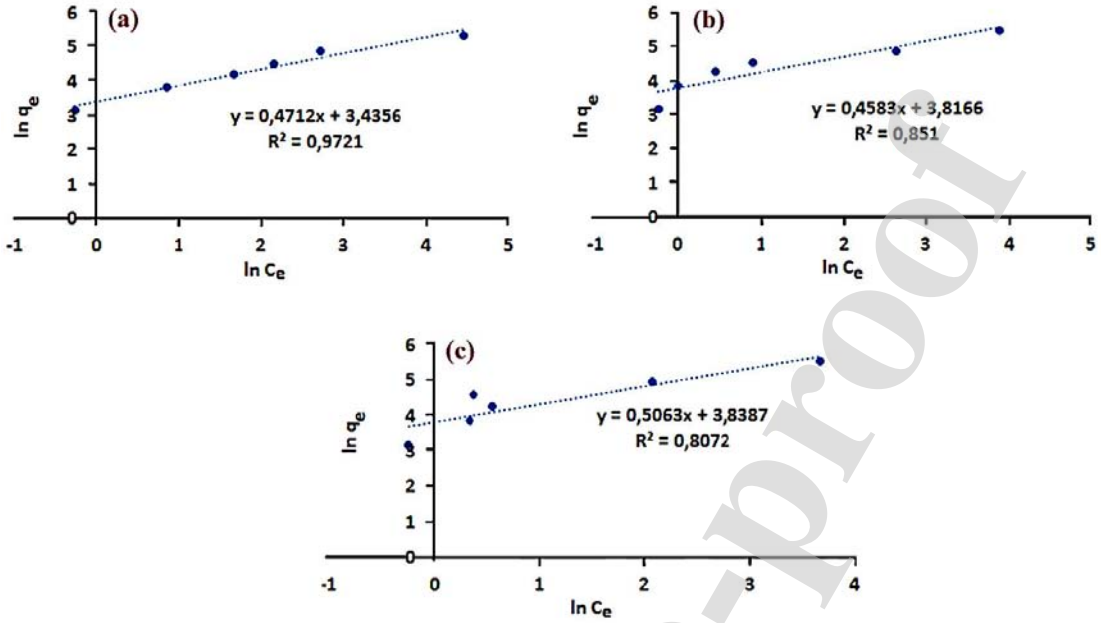

Figure 11. Freundlich isotherm plots obtained at **(a)** 298K, **(b)** 308K **(c)** 318K

The Freundlich parameters defined from the plot in **Figure 11** were given in **Table 2.** As seen from tabulated data, the correlation coefficient (R^2) was 0.80-0.97 for a temperature range of 298-318 K. This means that the adsorption equilibrium data was not adequately favorable by Freundlich isotherm model. By considering both isotherm modeling results, hence the elimination of MG with $Zn(OH)_2$-AC composite was carried out at a single layer and with electrostatic attraction power.

Table 2. Langmuir and Freundlich isotherm constants obtained for 298, 308 and 318 K.

Temperature (K)	Langmiur isotherm			Freundlich isotherm		
	q_m (mg/g)	K_L (L/mg)	R^2	K_F	n (l/mg)	R^2
298	243.90	0.09	0.99	31.19	2.12	0.97
308	277.78	0.15	0.95	45.60	2.18	0.85
318	303.03	0.15	0.97	46.53	1.97	0.80

3.9. Kinetic studies

The kinetic mechanism of MG adsorption was identified by pseudo 1st and 2nd order kinetic models. Pseudo 1st order model (Lagergren et al., 1898) was applied to the equilibrium data to

examine the adsorption mechanism. The linear form of Lagergre's equation was written as below:

$$\log(q_e - q_t) = \log(q_t) - \frac{k_1}{2{,}303} t \quad (10)$$

Here, q_e (mg.g^{-1}) and q_t (mg.g^{-1}) are the adsorbed amount of the adsorbate at equilibrium time and any t time and k_1 (min^{-1}) is rate constant. k_1 and q_e values are computed from slope and intersection point of the plot ln(q_e-q_t) vs t. Kinetic data obtained from pseudo 1st order modeling for initial MG concentration of 50, 100, and 150 mg L^{-1} is shown in **Table 3** and **Figure 12.**

On the other hand, the kinetic mechanism of MG adsorption onto Zn(OH)$_2$-AC composite was investigated using pseudo 2nd order model equation which is defined as below (Mckay and Ho, 1999):

$$\frac{t}{q_t} = \left[\frac{1}{k_2 q_e^2}\right] + \frac{1}{q_e} t \quad (9)$$

Here, k_2 (g.mg^{-1}.min^{-1}) is the constant of 2nd order rate constant. q_e and k_2 values are determined based on the plot of t/q_t vs t.

The R^2 values in the ranges of 0.98-0.99 demonstrated that pseudo 1st order kinetic model was not very appropriate to recognize MG adsorption mechanism onto Zn(OH)$_2$-AC composite, **Figure 13 and Table 3.** Besides, the $q_{e,exp}$ values for three initial concentrations were well agreement with the $q_{e,cal}$ values, hence the MG removal over Zn(OH)$_2$-AC composite can be better monitored by the 2nd order kinetic model.

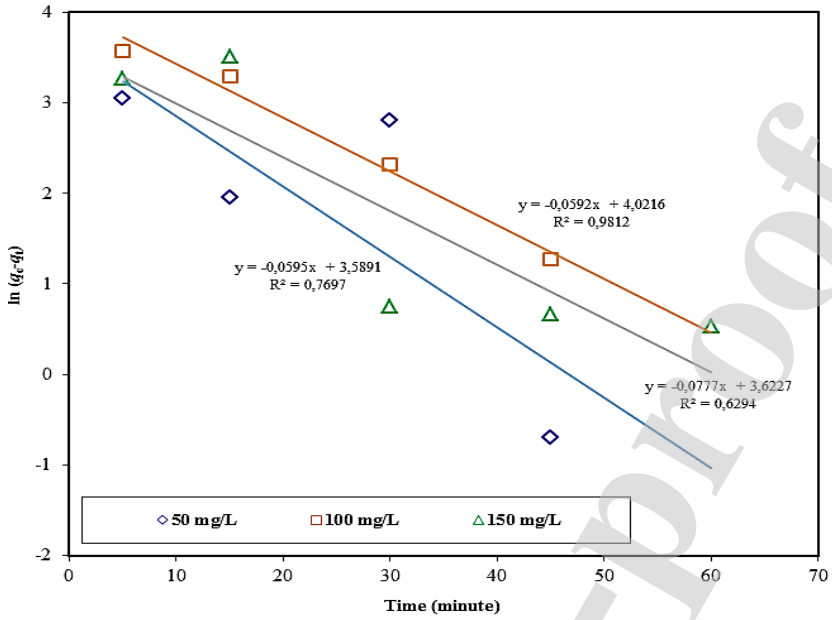

Figure 12. Pseudo 1st order kinetic modeling results obtained for MG adsorption onto $Zn(OH)_2$-AC composite (Initial MG concentration: 50, 100 and 150 mg/L, adsorbent dose: 0.1g/100 mL, pH: 7, temperature: 298 K).

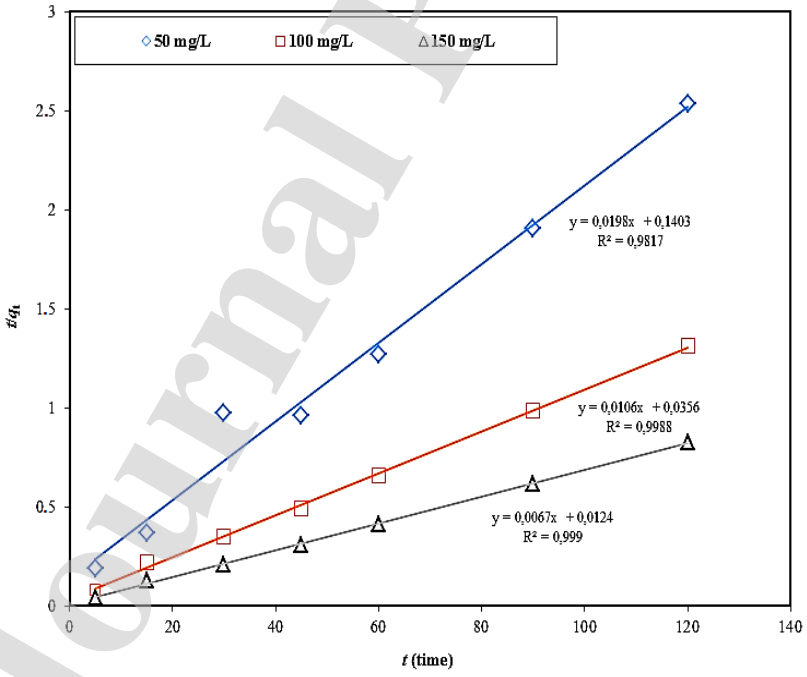

Figure 13. Pseudo 2nd order kinetic results obtained for MG adsorption onto $Zn(OH)_2$-AC composite (Initial MG concentration: 50, 100 and 150 mg/L, adsorbent dose: 0.1g/100 mL, pH: 7, temperature: 298K).

Table 3. Kinetic results determined based on pseudo 1st and 2nd order kinetic models

	Pseudo 1st order				Pseudo 2nd order		
C_0 (mg.L^{-1})	$q_{e\ exp}$	$k_{1,\ min}^{-1}$	$q_{e\ cal}$ (mg.g^{-1})	R^2	k_2 (g.mg^{-1}.min^{-1})	$q_{e\ cal}$ (mg.g^{-1})	R^2
50	47.66	0.17	36.20	0.63	0.141	50.51	0.98
100	91.30	0.14	37.44	0.98	0.297	94.33	0.98
150	134.81	0.13	55.79	0.77	0.540	149.25	0.99

3.10. Reusability study

The MG desorption efficiency was investigated using six different concentrated-eluents: 0.05 M NaOH, 0.1 M NaOH, 0.2 M NaOH, 0.05 M HCl, 0.1 M HCl and 0.2 HCl. The desorption efficiency was determined to be 83.62%, 88.3%, 97.6%, 87.22%, 89.90% and 93.45%, respectively. As can be seen from these results, the maximum desorption efficiency was achieved by using 0.2 M NaOH solution and therefore was selected as optimum eluent. The reusability was checked by following the adsorption–desorption process for 0.2 M NaOH eluent. On the other hand, reusability performance is one of the fundamental criteria of a freshly developed adsorbent in terms of reducing its utilization cost for engineering scale-wastewater cleaning processes. By considering this fact, a seven cycling-adsorption/desorption treatment was conducted to establish the reuse performance of $Zn(OH)_2$-AC composite adsorbent for the removal of MG from aquatic media. With this aim, desorption experiments were carried out using 0.05, 0.10, and 0.20 M NaOH. The reusability yield (%) for each cycle was shown in **Figure 14**. Only about 12%-reduction was occurred in adsorption yield during the first four cycles and it was reached to about 24% after 7th cycle although the desorption yield was almost constant. The reduction in the adsorption capacity of the composite adsorbent could be due to the partially deactivation of its adsorption cites during the cycling treatment. Consequently, the developed $Zn(OH)_2$-AC composite adsorbent demonstrated a reasonable reuse performance throughout the removal of MG from aqueous media.

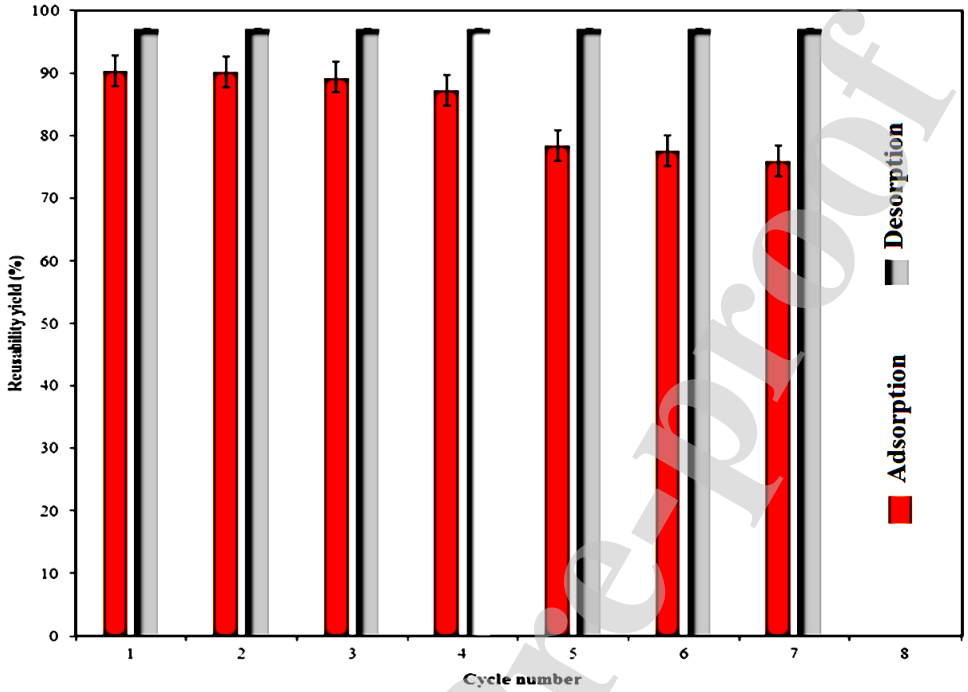

Figure 14. Reusability yield (%) for seven adsorption/desorption cycles (298 K, adsorbent dose: 0.10 g/0.1L, pH: 7)

3.11. Comparison of the developed adsorbent in terms of adsorption capacity

The MG removal performance of the synthesized $Zn(OH)_2$-AC composite adsorbent via ultrasonically assisted method with different kinds of adsorbents available in literature was compared in **Table 4.** As can be seen from the tabulated data, the adsorption capacity of the developed adsorbent is higher than most of the adsorbents. The results show that the produced $Zn(OH)_2$-AC composite adsorbent has a remarkable MG removal ability. This observation suggests that the increased adsorption capacity of ultrasonically assisted synthesis in MG removal may be caused by high pressure shock waves during the violent collapse of cavitation bubbles.

422 **Table 4.** Comparison of MG adsorption capacity of $Zn(OH)_2$-AC composite with that of
423 different kind of adsorbents reported in the literature

Adsorbent	pH	Temperature (K)	Synthesis Method	Adsorbent dose	Initial concentration (mg/L)	Adsorption capacity (mg/g)	Reference
Nano-ZnO/ pollen	6.6	298	Two-step liquid precipitation	0.05 g/mL	50	145.9	(Tzvetkov et al., 2017)
Fe-Zn nanoparticle	9	323	Coprecipitation	0.15g/50 mL	25-100	21.7	(Gautam et al., 2015)
ZnO-loaded AC	7	298	Microwave irradiation	15 mg/50 mL	5-30	59.17	(Azad et al., 2015)
$Zn(OH)_2$-NP-AC	4.5	298	Sonochemically	0.019 g/mL	20	74.63	(Bazrafshan et al., 2015)
Functionalized AC	8	298	Microwave-assisted	0.001 g/50 mL	25-65	333.3	(Ghasemi et al., 2016)
Chestnut shell-based AC	7	318	Carbonazition	0.1 g/100 mL	25-200	106.54	(Altintig et al., 2018)
Fe_3O_4-AC	7	318	Magnetic coating	0.1 g/100 mL	25-200	311.40	(Altintig et al., 2018)
AC/$CoFe_2O_4$	5	n.a	Facile refluxing	0.05 g/25 mL	n.a	89.29	(Ai et al., 2010)
$Zn(OH)_2$-AC composite	7	318	Ultrasonically	0.1 g/100 mL	25-300	303.0	*This study*

424

425 **4. Conclusions**

426 In this work, it is aimed to develop and characterize coffee waste-based activated carbon (AC)
427 as an eco-friendly and highly efficient material. The bio-based AC was doped ultrasonically
428 with $Zn(OH)_2$ and used successfully for the removal of MG from water. The studied pH,
429 temperature, adsorbent dose, and initial MG concentration affected the adsorption yield
430 remarkably effects. The adsorption equilibrium results were modeled with Langmuir and
431 Freundlich isotherms and the Langmuir model is the more suitable for recognize the sorption
432 type. The maximum adsorption capacity of the produced $Zn(OH)_2$-AC composite was
433 determined by the evaluation of linear Langmuir isotherm plot as 303.0 mg/g at 318 K and pH
434 7. Thermodynamic calculations displayed that the adsorption process had spontaneous and
435 endothermic character. The kinetic studies exposed that the pseudo 2nd order model was well
436 proper to identify the adsorption mechanism. The prepared adsorbent had outstanding

reusability performance after even the 7th cycle. The produced $Zn(OH)_2$-AC composite has good usage potential as an alternative adsorbent for the effective removal of MG from wastewaters because of its relatively high adsorption capacity, reasonable reuse performance, and being of cost-effective and eco-friendly.

References

Ahmad, M.A., Alrozi, R. (2011). Optimization of rambutan peel based activated carbon preparation conditions for Remazol brilliant blue removal, Chem. Eng. J., 168(1), 280–85.

Ai, L., Huang, H., Chen, Z., Wei, X., Jiang, J. (2010). Activated carbon/$CoFe_2O_4$ composites: Facile synthesis, magnetic performance and their potential application for the removal of malachite green from water, Chem. Eng. J., 156, 243–249.

Allen, S.J., Mckay, G., Porter, J.F. (2004). Adsorption isotherm models for basic dye adsorption by peat in single and binary component systems, J. Colloid Interf. Sci., 280(2), 322-333.

Almeida, C.A.P., Debacher, N.A., Downs, A.J., Cottet, L., Mello, C.A.D. (2009). Removal of methylene blue from colored effluents by adsorption on montmorillonite clay, J. Colloid Int. Sci., 332, 46-53.

Altintig, E., Onaran, M., Sarı, A., Altundag, H., Tuzen, M. (2018). Preparation, characterization and evaluation of bio-based magnetic activated carbon for effective adsorption of malachite green from aqueous solution, Mater. Chem. Phys., 220, 313-321.

Arias, F., Sen, T.K. (2009). Removal of zinc metal ion (Zn^{2+}) from its aqueous solution by kaolin clay mineral: a kinetic and equilibrium study, Colloid. Surface., 348, 100–108.

Asfaram, M., Ghadei, M., Agarwal, S., Tyagi, I., Gupta, V.K., (2015). Removal of basic dye Auramine-O by ZnS:Cu nanoparticles loaded on activated carbon: optimization of

462 parameters using response surface methodology with central composite design, RSC
463 Adv., 5, 18438-18450.
464 Askari, H., Ghadei, M., Dashtian, K., Azghandi, M.H.A. (2017). Rapid and high-capacity
465 ultrasonic assisted adsorption of ternary toxic anionic dyes onto MOF-5-activated
466 carbon: artificial neural networks, partial least squares, desirability function and
467 isotherm and kinetic study, Ultrason. Sonochem., 37, 71–82.
468 Azad, N.F., Ghadei, M., Dashtian, K., Hajati, S., Goudarzi, A., Jamshidi, M. (2015).
469 Enhanced simultaneous removal of malachite green and safranin O by ZnO nanorod-
470 loaded activated carbon: modeling optimization and adsorption isotherms, New
471 J.Chem.,39, 7998-8005.
472 Bazrafshan, A., Hajati, S., Ghaedi, M. (2015). Synthesis of regenerable $Zn(OH)_2$ nanoparticle-
473 loaded activated carbon for the ultrasound-assisted removal of malachite green:
474 optimization, isotherm and kinetics, RSC Adv., 5, 79119-79128.
475 Behzad, H., Susana, R.C., Mohammad, A.A., Mohammad, A., Inderjee, T.T., Shilpi, A.,
476 Vinod, K.G. (2015). Kinetics and thermodynamics of enhanced adsorption of the dye
477 ar18 using activated carbons prepared from walnut and poplar woods, J. Mol. Liq.
478 208, 99-105.
479 Breitbach, M., Bathen, D. (2001). Influence of ultrasound on adsorption processes, Ultrason.
480 Sonochem., 8, 277 – 283.
481 Dashamiri, S., Ghadei, M., Dashtian, K., Rahimi, M.R. Goudarzi, A., Jannesar, R. (2016).
482 Ultrasonic enhancement of the simultaneous removal of quaternary toxic organic dyes
483 by CuO nanoparticles loaded on activated carbon: central composite design, kinetic
484 and isotherm study, Ultrason. Sonochem., 31, 546–557.

Dawood, S., Sen, T.K. (2012). Removal of anionic dye Congo red from aqueous solution by raw pine and acid-treated pine cone powder as adsorbent: equilibrium, thermodynamic, kinetics, mechanism and process design, Water Res., 46, 1933-1946.

Dessyntha, K., Priwidyanjati, A. (2017). Adsorption of malachite green dye from aqueous solution on the bamboo leaf ash, AIP Conference Proceedings. 1911, 020011-7.

Feng, Y., Dionysiou, D.D., Wu, Y., Zhou, H., Xue, L., He, S., Yang, L. (2013). Adsorption of dyestuff from aqueous solutions through oxalic acid-modified swede rape straw: Adsorption process and disposal methodology of depleted bioadsorbents, Biores. Technol., 138, 191-197.

Gautam, R.K., Rawat, V., Banerjee, S., Sanroman, M.A., Soni, S., Sing, S.K., Chattopadhyaya, M.C. (2015). Synthesis of biometallic Fe-Zn nanoparticle and its application towards adsorptive removal of carcinogenic dye malachite green and Cango red in water, J. Mol. Liq., 212, 227-236.

Ghaedi, M., Khafri, H.Z., Asfaram, A., Goudarzi, A. (2016). Response surface methodology approach for optimization of adsorption of Janus Green B from aqueous solution onto $ZnO/Zn(OH)_2$-NP-AC: Kinetic and isotherm study, Spectrochim. Acta A. 152, 233–240.

Ghasemi, M., Mashhadi, S., Asif, M., Tyagi, I. (2016). Microwave-assisted synthesis of tetraethylenepentamine functionalized activated carbon with high adsorption capacity for Malachite green dye, J. Mol. Liq., 213, 317–325.

Gupta, S.S., Krishna, G.B. (2011). Kinetics of adsorption of metal ions on inorganic materials: A review, Adv. Colloid Interf. Sci., 162(1–2), 39–58.

Huang, Y.D. (2017). Comments on a novel magnetic chitosan/clinoptilolite/magnetite nanocomposite for highly efficient removal of Pb(II) ions from aqueous solution, Powder Technol., 324, 16-17.

Ip, A.W.M., Barford, J.P., McKay, G. (2009). Reactive black dye adsorption/desorption onto different adsorbents: effect of salt, surface chemistry, pore size and surface area, J. Colloid Interf. Sci., 337(1), 32-38.

Jing, G., Zhou, Z., Song, L., Dong, M. (2011). Ultrasound enhanced adsorption and desorption of chromium (VI) on activated carbon and polymeric resin, Desalination. 279, 423 – 427.

Khan, A.T., Rahman, R., Ali, I., Khan, E.A., Mukhlif, A.A. (2014). Removal of malachite green from aqueous solution using waste pea shells as low-cost adsorbent–adsorption isotherms and Dynamics, Toxicol. Environ. Chem., 96, 569-578.

Lagergren, S. (1898). Zur theorie der sogenannten adsorption geloster stöffe, Kungliga Sevenska Vetenskapsakademiens, Handlingar. 24, 1.

Lin, G., Wang, S.X., Zhang, L.B., Hu, T., Peng, J.H., Cheng, S., Fu, L.K. (2017). Selective adsorption of Ag^{+} on a new cyanuric-thiosemicarbazide chelating resin with high capacity from acid solutions, Polymer. 9, 568.

Liu, Z., Zhou, X., Wu, F., Liu, Z. microwave-assisted preparation of activated carbon modified by zinc chloride as a packing material for column separation of saccharides, ACS Omega. 2020, 5, 10106−10114.

Mazaheri, H., Ghaedi, M., Hajati, S., Dashtian, K., Purkait, M.K. (2015). Simultaneous removal of methylene blue and Pb^{+2} ions using ruthenium nanoparticle-loaded activated carbon:response surface methodology, RSC Adv.,5, 83427-83435.

Mckay, G., Ho, Y.S. (1999). Pseudo-Second Order Model for Sorption Process. 34, 451-465.

Mosayebi, E., Azizian, S., Hajian, A. (2015). Synthesis of nanostructured and microstructure ZnO and $Zn(OH)_2$ on activated carbon cloth by hydrothermal and microwave-assisted chemical bath deposition methods, Superlattices Microst., 81, 226-232.

534 Mosayebi, E., Azizian, S. (2016). Study of copper ion adsorption from aqueous solution with
535 different nanostructured and micro structured zinc oxides and zinc hydroxide loaded
536 on activated carbon cloth, J. Mol. Liq., 214, 384-389.
537 Ozdemir, Y., Dogan, M., Alkan, M. (2006). Adsorption of cationic dyes from aqueous
538 solutions by sepiolite, Microporous Mesoporous Mat., 96, 419-427.
539 Pereira, M.F.R., Soares, S.F., Orfao, J.J.M., Figueiredo, J.L. (2003). Adsorption of dyes on
540 activated carbons: influence of surface chemical groups, Carbon. 41, 811–821.
541 Ramaraju, B., Reddy, P.M.K., Subrahmanyam, C. (2014). Low cost adsorbents from
542 agricultural waste for removal of dyes, Environ. Prog. Sustain. Energy, 33, 38–46.
543 Sadeghi, O., Amini, M.M., Bazargani, M.F.B., Mehrani, A.,Aghabali, A., Adineh, M., Amani,
544 V., Mehrani K. Immobilization of metalloporphyrin on functionalized magnetic
545 nanoparticles as a catalyst in oxidation of cyclohexene: novel modified Fe3O4 nanoparticles
546 with triethoxysilane agent. J. Inorg. Organomet. Polym. Mater., 22 (2012), pp. 530-535.
547 Sara, D., Tushar, K.S. (2012). Removal of anionic dye congo red from aqueous solution by
548 raw pine and acid-treated pine cone powder as adsorbent: equilibrium,
549 thermodynamic, kinetics, mechanism and process design, Water Res., 46, 1933–1946.
550 Sartapea, A.S., Mandharea, A.M., Jadhavb, V.V., Rautb, P.D., Anusea, M.A., Kolekar, S.S.
551 (2017). Removal of malachite green dye from aqueous solution with adsorption
552 technique using Limonia acidissima (wood apple) shell as low-cost adsorbent, Arab. J.
553 Chem., 10, 3229–3238.
554 Senthilkumaar, S., Kalaamani, P., Porkodi, K., Varadarajan, P.R., Subburaam, C.V. (2006).
555 Adsorption of dissolved reactive red dye from aqueous phase onto activated carbon
556 prepared from agricultural waste, Bioresource Technol., 97(14), 1618–1622.

557 Senthilkumaar, S., Varadarajan, P.R., Porkodi, K., Subbhuraam, C.V. (2005). Adsorption of
558 methylene blue onto jute fiber carbon: kinetics and equilibrium studies, J. Coll. Int.
559 Sci., 284, 78-82.
560 Sharma, P., Kaur, H., Sharma, M., Sahore, V. (2011). A review on applicability of naturally
561 available adsorbents for the removal of hazardous dyes from aqueous waste, Environ.
562 Monit. Assess., 183, 151–195.
563 Sharma, A., Singh, P.B., Dhar, S., Gondorf, A., Spasova, M. (2012). Effect of surface groups
564 on the luminescence property of ZnO nanoparticles synthesized by sol-gel route, Surf.
565 Sci., 606, 13-17.
566 Sohail, A., Faraz, M., Arif, H., Bhat, S.A., Siddiqui, A.A., Bano, B. (2017). Deciphering the
567 interaction of bovine heart cystatin with ZnO nanoparticles: Spectroscopic and
568 thermodynamic approach, Int. J. Biological Macromol., 95, 1056–1063.
569 Tzvetkov, G., Kaneva, N., Spassov, T. (2017). Room-temperature fabrication of core-shell
570 nano-ZnO/pollen grain biocomposite for adsorptive removal of organic dye from
571 water, Applied Surf. Sci., 400, 481–491.
572 Walker, G.M., Weatherley, L.R. (1997). Adsorption of acid dyes onto granular activated
573 carbon in fixed beds, Water Res., 31(8), 2093-101.
574 Wangi, S., Zhu, Z.H. (2007). Effects of acidic treatment of activated carbons on dye
575 adsorption, Dyes Pigments. 75, 306–314.
576 Wang, C., Wang, F., Xu, M., Zhu, C., Fang, W., Wei, Y. (2015). Electrocatalytic degradation
577 of methylene bulue on Co doped Ti/TiO_2 nanotube/PbO_2 anodes prepared by pulse
578 electrodeposition, J. Electroanal. Chem., 759, 156-166.
579 Wang, G., Yang, L., Jiang, L., Shi, M., Wei, Z., Zhong, W., Li, S., Cui, J., Wei, W. (2016).
580 Simple combination of humic acid with biogenic hydroxyapatite achieved highly

efficient removal of methylene blue from aqueous solution, RSC Adv., 6, 66888-67897.

Xiao, X., Luo, S., Zeng, G., Wei, W., Wan, Y., Chen, L., Gou, H., Cao, Z., Yang, L., Chen, J., Xi, Q. (2010). Biosorption of cadmium by endophytic fungus (ef) microshaeropsis sp. lse10 isolated from cadmium hyperaccumulator solanum nigrum l., Biosesource Technol., 101, 1668-1674.

Yu, M., Han, Y., Li, J., Wang, L. (2017). CO_2-activated porous carbon derived from cattail biomass for removal of malachite green dye and application as supercapacitors, Chem. Eng. J., 317, 493–502.

Zhang H.M. , Ruan Y. , Liang A.P. , Shih K.M. , Diao Z. H, , Su M.H., Hou L.A., Chen D.Y., Lu H., Kong L.J., (2019) Carbothermal reduction for preparing nZVI/BC to extract uranium: insight into the iron species dependent uranium adsorption behavior, J. Clean. Prod., 239, 117873.

Zhu K. , Song G. , X Chen Ren. , C. , (2020) Solvent-free engineering of Fe0/Fe3C nanoparticles encased in nitrogen-doped carbon nanoshell materials for highly efficient removal of uranyl ions from acidic solution, J. Colloid Interf. Sci., 575, 16-23.

Saleh, T.A., (2020) Nanomaterials: Classification, properties, and environmental toxicities, Environmental Technology & Innovation, 20 (2020) 101067, doi.org/10.1016/j.eti.2020.101067

Saleh, T.A. (2020) Trends in the sample preparation and analysis of nanomaterials as environmental contaminants, Trends in Environmental Analytical Chemistry, 28, e00101, doi.org/10.1016/j.teac.2020.e00101

Highlights

- AC sorbent was produced from coffee waste with low cost material.
- AC/zinc hydroxide nanoparticles composite was used to remove MG from aqueous solutions.
- The dependency of the adsorption efficiency on the batch parameters was studied.
- The maximum adsorption capacity was determined to be 303.03 mg g^{-1}
- The synthesized adsorbent can be promising sorbent for MG elimination from wastewaters.

GRAPHICAL ABSTRACT

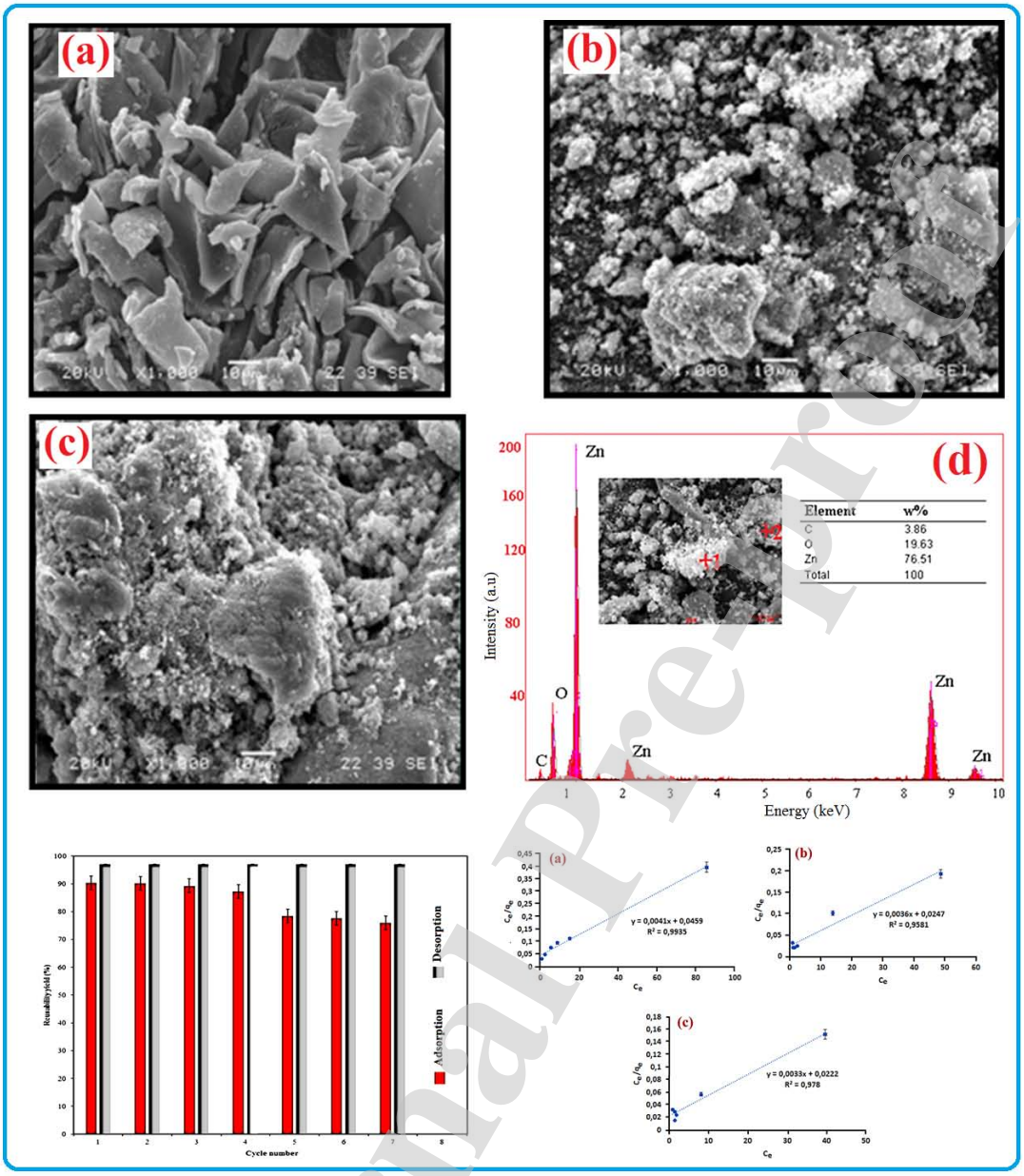

Notes

The authors declare no competing financial interest.

Author contribution

Esra Altıntıg: performed the experiments and results with draft writing.

Merve Yenigun: performed the experiments and results with draft writing.

Ahmet Sarı: reviewed the paper, supervision and checked the manuscript.

Huseyin Altundag: performed experiments and results.

Mustafa Tuzen: reviewed the paper, supervision and checked the manuscript.

Tawfik A. Saleh: reviewed the paper, supervision and checked the manuscript.

Declaration of interests

☒ The authors declare that they have no known competing financial interests or personal relationships that could have appeared to influence the work reported in this paper.

☐The authors declare the following financial interests/personal relationships which may be considered as potential competing interests: